Fundamental Researches of an Electron Gun with Field Emitter

Fundamental Researches of an Electron Gun
with Field Emitter

Koichi NAGAMI*

As fundamental researches for the purpose of applying the field emitter to the electron gun producing the fine electron beam, the stability of the emission and the field distributions with specified electrode structures are studied. The field emitter is able to operate in the stable state of d.c. emission at higher temperature than about 1,000°C, even if the vacuum degree is in the order of 10^{-5} mmHg. Analyses on the field distributions give the basic data for constructing the electrodes and determining the operating voltage in the practical electron gun with field emitter. Measurements by making use of the experimental device are also described, and show the results agreeing with the fundamental researches.

1. Introduction

This paper treats of the fundamental researches developed with the intention of applying field emitter to the electron gun producing the fine electron beam. Field emitters have unique electrical properties suitable for producing the fine electron beam. Notably among such properties are these: the enormous current density exceeds that obtained by the ordinary thermionic emission; the emitters may operate at room temperature or at lower temperature than that of other conventional emitters; the minute emitting surface provides a virtual point source useful in electron optical devices.

The emission current density obtained by pure field emission is given by the Fowler-Nordheim equation,[1,2] when the metal temperature is assumed zero and no electron surmounts the potential barrier at the metal surface. Lately Nakai,[3] and Dolan and Dyke[4] calculated the emission current density under the conditions that field strength at the metal surface and the metal temperature are both high enough to permit appreciable emission both over and through the potential barrier. The descriptive term T-F emission has been applied to this case. And other studies on the field emission such as the stability of the emission due to the surface state of the emitter and the field emission microscope have also been reported.[5]

Further researches, however, toward the practical application of the field emitter to the electron gun are necessary. Among these are the researches on the stability of the emission under the pressure expected in the practical devices and on the electrode design from which the field distribution over the emitter surface and the electron trajectories are determined.

2. Stability of Emission

The field emission current I, obtained by integrating the Fowler-Nordheim equation

---

* Department of Electronic Engineering, College of Engineering.

over the total emitting area A, is expressed by

$$I=\int_0^A 1.54\times10^{-6}\frac{(KV)^2}{\phi}\exp\left[-6.83\times10^7\phi^{3/2}\frac{f(y)}{KV}\right]dA \qquad (1)$$

where

$$F=KV \qquad (2)$$

and F is field strength at the emitter surface in volts/cm, V is anode voltage in volts, K is a geometrical factor in cm^{-1}, ϕ is work function of the emitter in eV, and $f(y)$ is a dimensionless elliptic function of the variable $y=3.79\times10^{-4}\,F^{1/2}/\phi$.

The experiments on the stability of the current-voltage characteristics of the field emission at various pressures were performed by making use of the device shown in Fig. 1. The device can be evacuated to the order of 10^{-10} mmHg by the action of ion pump after sufficient outgassing, and then O_2 gas is permeated into the device at any pressure from Ag tube by heating it, and alternatively H_2 gas also done from Pd tube by heating it in the atmosphere of H_2 gas. As the emitter has to be constructed in a needlelike shape in order to keep the value of K in Eq. (2) large, it is made from a fine tungsten wire, spot-welded to the supporting filament, by electrolytic etching in the NaOH 5% solution.

(a) Schematic diagram of the experimental device.
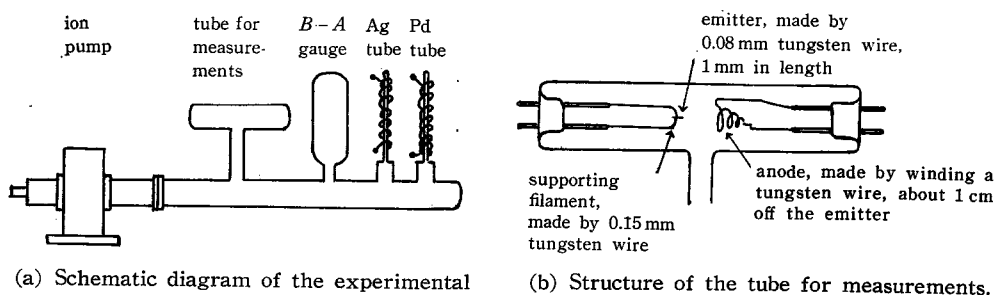
(b) Structure of the tube for measurements.

Fig. 1. Schematic diagram of the experimental device for measuring the emission stability.

Examples of the experimental results on the current-voltage characteristics at the stable state of d.c. emission are shown in Fig. 2. The slope of this graph depends on K and ϕ as mentioned in following equation,

$$\frac{d\log_{10}(I/V^2)}{d(1/V)}=-2.96\times10^7\frac{\phi^{3/2}}{K} \qquad (3)$$

which is derived from Eq. (1), assuming that the emitting area A is constant and the term deduced from $f(y)$ is put to unity as it is close to unity for the ranges of field strengths and work functions encountered in these experiments. From the values of K, $6.02\times10^3\,cm^{-1}$, calculated from the slope of curve 1 in Fig. 2 by putting ϕ at 4.5 eV for clean tungsten, and V used in the experiments, the values of field strengths at the emitter surface can be estimated by Eq. (2) to be in the range 2.8×10^7 V/cm$<F<6.5\times10^7$ V/cm. When F becomes more than the latter value, the d.c. emission cannot stay in the stable state due to so-called build-up and vacuum arc phenomena.
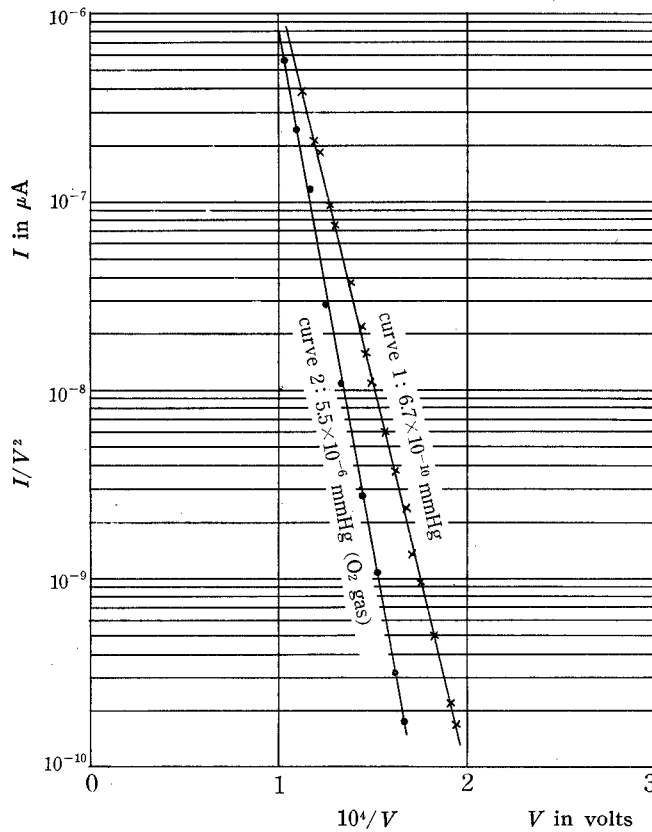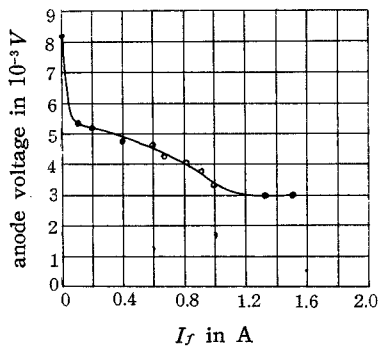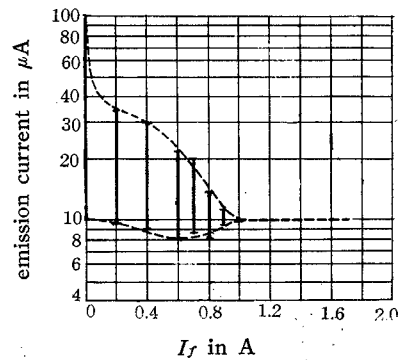
Fig. 2. Current-voltage chracteristics measured with an emitter at room temperature for different pressures.

(a) Variation of anode voltage needed for producing the average emission current, 10 μA

(b) Ranges of variation of the emission current measured in 30 second at a fixed anode voltage, 3 kV

Fig. 3. Examples of the unstabilities of the current-voltage characteristics as functions of the heating current I_f through the supporting filament, at high pressure, 2.5×10^{-5} mmHg, due to the presence of O_2 gas.

The experimental results on the emission stability, being much important for the present purpose, are illustrated in Fig. 3. The emitter temperature corresponding to the

heating current I_f through the supporting filament are calibrated by optical pyrometer, e.g. $T \simeq 1,000°C$ at $I_f = 1.0$ A. It is seen that at high pressure, shown in Fig. 3, due to the presence of O_2 gas, the emission stability cannot be experienced if $T < 1,000°C$, because the surface states of the emitter are affected by gas particles and cannot be held in the equilibrium condition under the migration effects due to both temperature and field. The similar situations are also experienced when H_2 gas is permeated into the device in place of O_2 gas. It is thus concluded that at lower vacuum degree than about 10^{-5} mmHg the emission stability can be maintained by keeping the emitter temperature over about $1,000°C$, i.e. under the condition of T$-$F emission.

3. Potential and Field Distributions

As the emitter tip is minute and its shape cannot always be controlled correctly through the manufacturing process mentioned above, the analyses of the field distribution are carried out based on the both cases of the electrode structures causing (I) spherical equipotential surfaces, and (II) rotationally paraboloidal equipotential surfaces, shown in Fig. 4 (a) and (b), respectively. Taking the center point of curvature at the axial point on the cathode surface as the origin for the coordinate in both cases, the axial potential
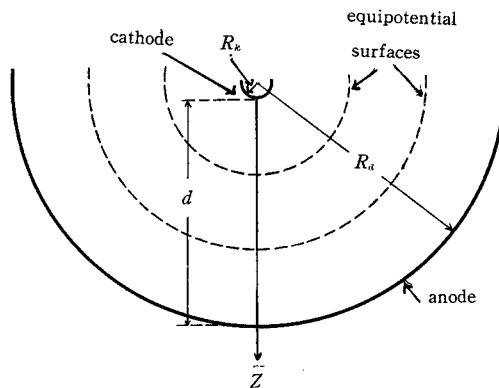
(a) Assumed electrode structure causing the spherical equipotential surfaces
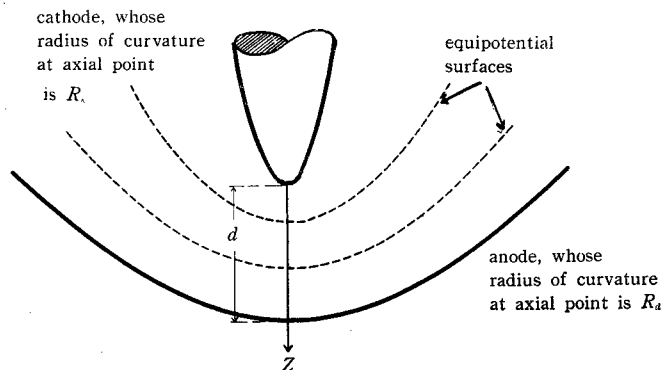
(b) Assumed electrode structure causing the rotationally paraboloidal equipotential surfaces
Fig. 4. Assumed electrode structures for bases of the analyses of the field distributions.

V_r of any equipotential surface, whose radius of curvature at the axial point on each surface is r, are given by following equations

$$\frac{V_r}{V_d}=\frac{1}{1-n}\left\{1-\frac{n}{(r/R_d)}\right\} \qquad \text{for case I} \qquad (4)$$

$$\frac{V_r}{V_d}=1-\frac{\ln(r/R_d)}{\ln n} \qquad \text{for case II} \qquad (5)$$

where

$$n=R_k/R_d \qquad \text{for both cases} \qquad (6)$$

and V_d is the anode potential with respect to the cathode potential. If the origin is shifted to the axial point on the cathode surface, the potential distribution V_z along the axis are rewrited as follows

$$\frac{V_z}{V_d}=\frac{1+m}{1+\{m/(z/d)\}} \qquad \text{for case I} \qquad (7)$$

$$\frac{V_z}{V_d}=\frac{\ln\{1+(2/m)(z/d)\}}{\ln\{1+(2/m)\}} \qquad \text{for case II} \qquad (8)$$

where

$$m=R_k/d \qquad \text{for both cases} \qquad (9)$$

The axial field strength at the axial point on the cathode surface, F_{zk}, can be deduced from Eq. (7) or (8) as follows

$$\frac{F_{zk}}{F_{mean}}=1+(1/m) \qquad \text{for case I} \qquad (10)$$

$$\frac{F_{zk}}{F_{mean}}=\frac{2/m}{\ln\{1+(2/m)\}} \qquad \text{for case II} \qquad (11)$$

where

$$F_{mean}=-V_d/d \qquad \text{for both cases} \qquad (12)$$

Calculations from Eqs. (10) and (11) for various values of m give the results shown in Table 1. It is seen that in order to give $F_{zk}=3\times10^7$ V/cm, which is a reasonable value for producing appreciable emissions, when $d=1$ cm in case II, $V_d=218$ V if $R_k=10^{-6}$ cm, and $V_d=1830$ V if $R_k=10^{-5}$ cm.

Table. 1. Field strengths at the axial point on the emitter surface, calculated from Eqs. (10) and (11).

$m=R_k/d$	F_{zk}/F_{mean}	
	Case I, shown in Fig. 4 (a) and Eq. (10)	Case II, shown in Fig. 4 (b) and Eq. (11)
10^{-1}	1.1×10	6.57
10^{-2}	1.01×10^2	3.77×10
10^{-3}	10^3	2.63×10^2
10^{-4}	10^4	2.02×10^3
10^{-5}	10^5	1.64×10^4
10^{-6}	10^6	1.38×10^5
10^{-7}	10^7	1.19×10^6

It can be proved by the field plottings obtained by the resistance network analog system that the fields near the emitter surface are considered to be in more conformity with the ones obtained in case II than that in case I, even if the anode has a sphere-shaped surface. Fig. 5 shows the potential distributions along the axis, measured by the resistance network analog system or calculated from Eqs. (4) and (5). The field plotting is performed at first by representing the emitter by a line connecting several points on the axis of the resistance network, and the anode by a sphere-shaped electrode model whose radius is 20 meshes on the network, and attains to the result shown in curve 1 in Fig. 5. Curves 2 and 3 in Fig. 5 are the second and the third approximations, respectively, measured by enlarging the region between the emitter and a known equipotential surface gained in the previous plotting. The terminals of each curve correspond to the mesh points being 1 mesh off the emitter tip on the axis of the network. It is necessary to improve the approximation in order to know the field distributions on and near the emitter surface,
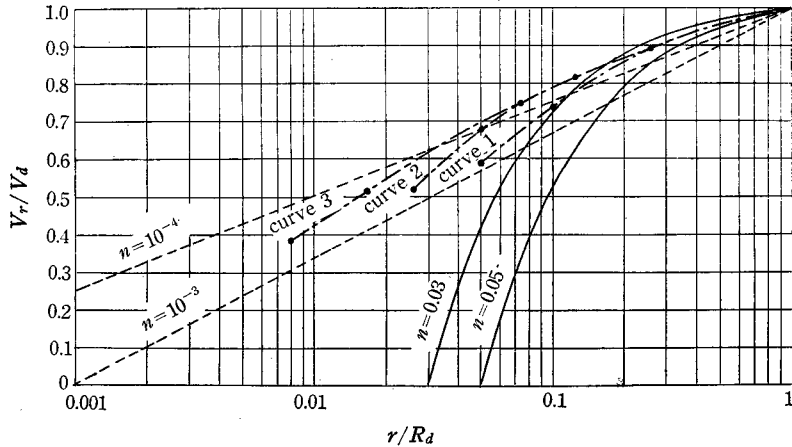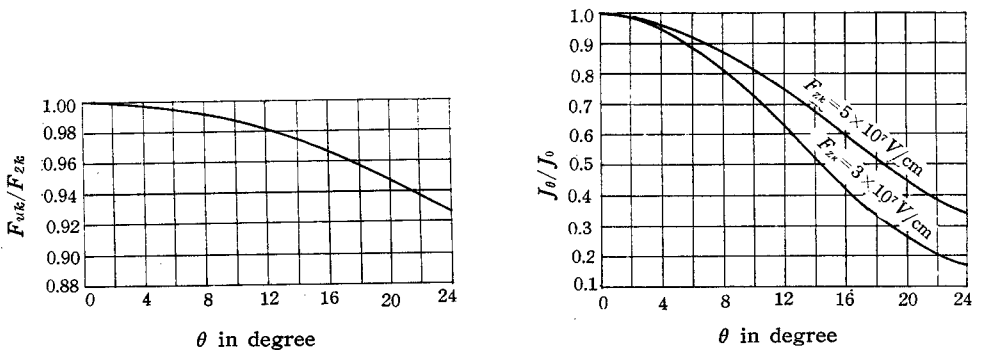

Fig. 5. Potential distributions along the axis as functions of r/R_d. Curves 1, 2 and 3 are the distributions measured by the resistance network analog system. The distributions calculated from Eqs. (4) and (5) are shown in solid and dotted curves, respectively, for ready comparison.

(a) Variation of field strengths   (b) Variation of emission current densities

Fig. 6. Variations of field strengths and field emission current densities on the surface of the rotationally paraboloidal emitter.

while the errors are accumulated by repeating the above procedure.

In case II, the field strengths, F_{uk}, being normal to the emitter surface at any point on the surface, differ from the one, F_{zk}, at the axial point on the surface. Analyses on this fact give the result shown in Fig. 6 (a). θ in the abscissa are angles between the axis and the lines from the center point of curvature at the axial point to any points on the surface. Curves in Fig. 6 (b) are calculated from the Fowler-Nordheim equation, and give the ratio of J_θ, the emission current density at the points on the surface corresponding to the given values of θ, to J_0, the one at the axial point.

4. Measurements by the Experimental Device

The experimental device for the electron gun with the field emitter is shown in Fig. 7. The device is demountable and its electrodes are made by stainless steel, except for the emitter. The value at which the pressure arrived in the device is 7×10^{-5} mmHg after pumping and outgassing. The tungsten emitter is manufactured by the process mentioned above, but 0.2 mm tungsten wire is used for the sakes of rigidity and stability. The anode has sphere-shaped inner surface, whose radius is 1 cm, in agreement with above discussions, and at the center point of curvature of it the emitter tip is positioned. The size of apertures in the anode structure are determined so small that the field near the emitter is not disturbed by them. The emitter temperature can be measured by optical pyrometer through the glass window and the aperture for observation. The auxiliary filament serves for bombarding the anode by electrons emitted from it. Electrons, emitted from
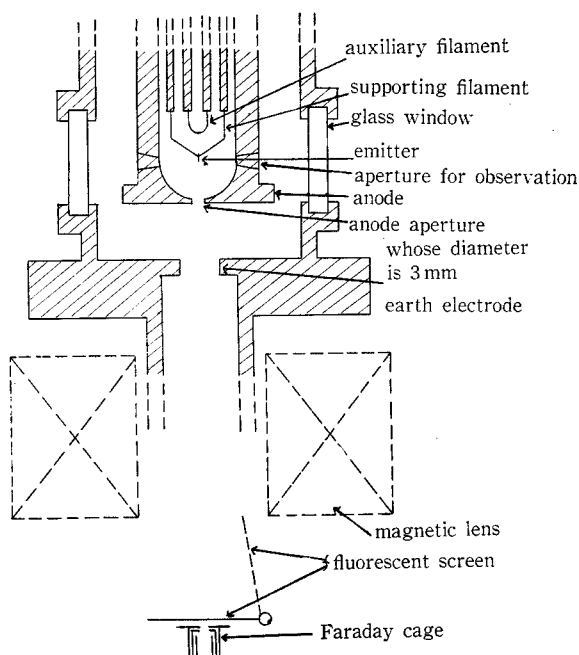
Fig. 7. Schematic diagram showing the cross sections of principal parts of the experimental device for the electron gun with field emitter.

the emitter in negative high potential, accelerated by the anode voltage V_d, and then passing through the anode aperture are focussed by the lens on the fluorescent screen, where the minute spot is observed, or into the Faraday cage if the screen is removed, which serves to measure the electron beam current I_b. The emitting area contributing to the beam current is estimated by

$$A = 2\pi R_k^2 (1 - \cos \theta_a) = 0.074 R_k^2 \qquad (13)$$

since the angle θ_α between the axis and the line from the apex of the emitter to the circumference of the anode aperture is so small and equal to $8°36'$ in this device.

The beam current-anode voltage characteristics measured with the emitter at room temperature are often unstable, but reliable data can be sometimes gained as shown in Fig. 8. In these curves corresponding to the individual emitters used in each measurement, it is seen that the emitter having larger value of K shows the characteristics whose slope is less steep, and is permitted to operates in lower range of the anode voltage, assuming that the value of work function is common for each emitter. Some quantities measured or estimated with ϕ taken as 4.5 eV are summarized in Table 2 for each curve shown in Fig. 8. Among these quantities, both V_d and I_b are measured values in each curve, K is calulated from the slope of each curve, F and J_F are done from Eq. (2) and the Fowler-Nordheim equation, respectively, A is estimated by $A=I_b/J_F$, and R_k is a approximate value estimated by Eq. (13) and a moderate value of A. The variations of the values of A in each case are due to the experimental errors and the assumptions used through the above estimations. These results show fairly well agreements with discussions in the above sections.

When the emitter is heated to higher temperature exceeding about 2,000°C, the beam current-anode voltage characteristics become quite stable, and thereafter they maintain the stable states without regard to the temperature variation down to about 1,000°C, below which, however, the unstabilities are again experienced. These phenomena coincide completely with the experimental results in the above section. Examples of the beam current-anode voltage characteristics measured with an emitter at the stable state of d.c. emission for various temperature higher than about 1,000°C are shown in Fig. 9, which are quite
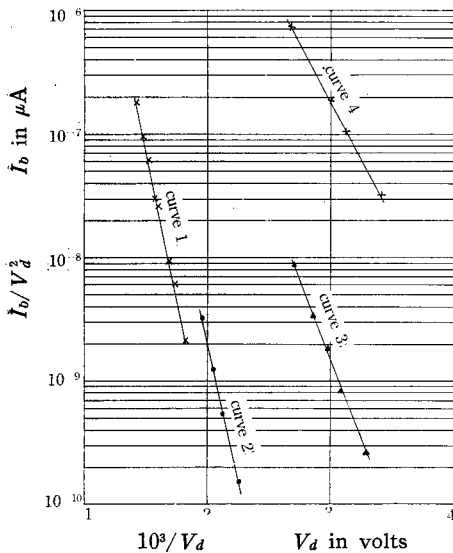

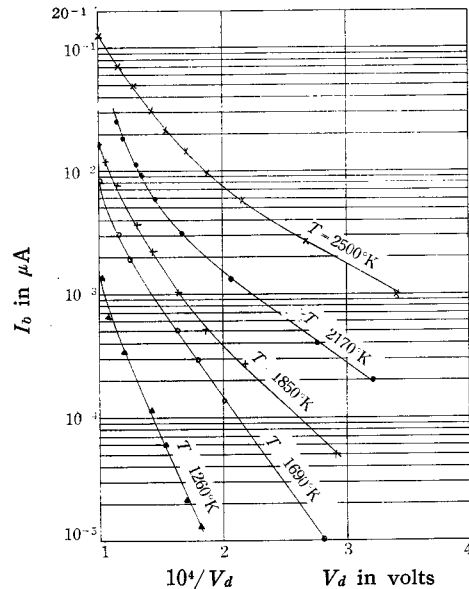Fig. 8. Beam current-anode voltage characteristics measured with various emitters at room temperature.

Fig. 9. Beam current-anode voltage characteristics measured with an emitter for various temperatures.

Table 2. Some quantities measured and estimated for various emitters corresponding to the curves in Fig. 8.

Quantities	Curve 1	Curve 2	Curve 3	Curve 4
Measured range of anode voltage V_d in V	545~700	430~510	310~370	300~375
Value of K in cm^{-1}	5.53×10^4	6.55×10^4	1.02×10^5	1.28×10^5
Field strength on emitter surface F in V/cm	3.01×10^7 $\sim 3.84 \times 10^7$	2.82×10^7 $\sim 3.34 \times 10^7$	3.16×10^7 $\sim 3.77 \times 10^7$	3.84×10^7 $\sim 4.80 \times 10^7$
Emission current density J_F in A/cm^2	4.2×10 $\sim 6.2 \times 10^3$	$9.0 \sim 4.0 \times 10^2$	1.4×10^2 $\sim 4.5 \times 10^3$	6.2×10^3 $\sim 2.4 \times 10^5$
Measured range of beam current I_b in A	7.0×10^{-10} $\sim 9.0 \times 10^{-8}$	1.1×10^{-11} $\sim 8.5 \times 10^{-10}$	2.5×10^{-11} $\sim 1.2 \times 10^{-9}$	3.0×10^{-9} $\sim 1.0 \times 10^{-7}$
Emitting area A in cm^2	1.5×10^{-11} $\sim 1.7 \times 10^{-11}$	1.2×10^{-12} $\sim 2.1 \times 10^{-12}$	1.7×10^{-13} $\sim 2.7 \times 10^{-13}$	4.2×10^{-13} $\sim 5.0 \times 10^{-13}$
Radius of curvature of emitter tip R_b in cm	1.5×10^{-5}	4.7×10^{-6}	1.7×10^{-6}	2.5×10^{-6}

similar to the results obtained by calculations under T−F emission. Considering the facts that the characteristics for various emitters are very analogous to each other and much higher values of the anode voltage are necessary for yielding the measurable beam current than the values with emitters at room temperature, one may infer that the various emitters are dulled by surface migration at high temperature to nearly a common tip radius, which is larger than each initiative value and estimated to be at severals of 10^{-5} cm.

5. Conclusions

It is proved that the field emitter is able to operates in the stable state of d.c. emission at higher temperature than about 1,000°C, even if the vacuum degree is in the order of 10^{-5} mmHg. The fields near the emitter are analyzed in the cases of electrode structures yielding both the spherical equipotential surfaces and the rotationally paraboloidal ones, and it is considered that the fields obtained in the latter case are in good comformity with the actual fields. Measurements with the experimental device show the results agreeing with these fundamental researches. The fundamentals for producing the electron gun with field emitter are established by the above results.

Acknowledgement

References

1) R. H. Fowler and L. W. Nordheim, Proc. Roy. Soc., **A119**, 173 (1928).
2) L. W. Nordheim, Proc. Roy. Soc., **A121**, 626 (1928).
3) J. Nakai, Tech. Rep. of the Osaka Univ., **vol. 1,** (1951).
4) W. W. Dolan and W. P. Dyke, Phys. Rev., **95**, 327 (1954).
5) W. P. Dyke and W. W. Dolan, Field Emission, Advances in Electronics and Electron Physics, vol. VIII. (1956).